Fiber breakage in polymer-matrix composite during static and fatigue loading, observed by electrical resistance measurement

Xiaojun Wang and D.D.L. Chung
Composite Materials Research Laboratory, State University of New York at Buffalo, Buffalo, NY 14260-4400

(Received 7 June 1999; accepted 25 August 1999)

By measuring the electrical resistance of a continuous unidirectional carbon fiber epoxy-matrix composite along the fiber direction during loading in this direction, fiber breakage was progressively monitored in real time. Fiber breakage occurred in spurts involving 1000 or more fibers. It started at about half of the failure strain during static tensile loading and at about half of the fatigue life during tension–tension fatigue testing. Immediately before static failure, at least 35% of the fibers were broken. Immediately before fatigue failure, at least 18% of the fibers were broken. The fiber breakage was accompanied by decrease in modulus.

I. INTRODUCTION

Continuous fiber polymer-matrix composites are used in aerospace, automobile, marine, machinery and construction industries, due to their low density, high strength, and high modulus. These composites degrade during loading due to fiber breakage, delamination, and other mechanisms that occur prior to failure. Because the degradation can render the composites unreliable or unsuitable for structural use, it is important to characterize and understand the degradation as it evolves during loading. For this purpose, real-time nondestructive monitoring of the degradation is needed. Techniques for this monitoring include acoustic emission detection,[1–4] eddy current testing, and the use of optical fiber sensors.[5] In the case of the fibers being electrically conducting and the matrix being insulating, electrical resistance measurement in the fiber direction of the composite provides a way to monitor damage in the form of fiber breakage, because fiber breakage causes the resistance of the composite in the fiber direction to increase.[6–10] By using this technique, we have monitored a continuous carbon-fiber polymer-matrix composite, during static and fatigue loading until failure, thereby obtaining information on the evolution of fiber breakage from its onset to composite failure. Prior work did not follow the entire fatigue process at a fixed stress amplitude and did not interpret the resistance changes to obtain the fraction of fibers broken.[6–10] Prior work[6–10] used the two-probe method for electrical resistance measurement, whereas this work used the four-probe method. The two-probe method suffers from the fact that the measured resistance includes the resistance of the electrical contacts, whereas the four-probe method excludes the contact resistance from the measured resistance. Nevertheless, the results of this work are consistent with those of prior work.

II. EXPERIMENTAL METHODS

Composite samples were constructed from individual layers cut from a 12-in.-wide unidirectional carbon-fiber prepreg tape manufactured by ICI Fiberite (Tempe, AZ). The product used was Hy-E 1076E, which consisted of a 976 epoxy matrix and 10E carbon fibers. The fiber and matrix properties are shown in Table I.

The composite laminates were laid up in a 4 × 7 in. platten compression mold with laminate configuration $[0]_8$ (i.e., eight unidirectional fiber layers in the laminate). The individual 4 × 7 in. fiber layers were cut from the prepreg tape. The layers were stacked in the mold with a mold release film on the top and bottom of the layup. No liquid mold release was necessary. The density and thickness of the laminate were 1.52 ± 0.01 g/cm^3 and 1.1 mm respectively. The volume fraction of carbon fibers in the composite was 58%. The laminates were cured using a cycle based on the ICI Fiberite C-5 cure cycle. The curing occurred at 355 ± 10 °F (179 ± 6 °C) and 89 psi (0.61 MPa) for 120 min. Afterward, they were cut to pieces of size 160 × 14 mm. Hence, each specimen had 38 bundles of fibers (6000 fibers per bundle, 7-μm diameter for each fiber). Glass-fiber-reinforced epoxy end tabs were applied to both ends on both sides of each piece, such that each tab was

30 mm long and the inner edges of the end tabs on the same side were 100 mm apart and the outer edges were 160 mm apart.

The electrical resistance R was measured in the longitudinal (fiber) direction using the four-probe method while either static or cyclic tension was applied in this direction. Silver paint was used for all electrical contacts. The four probes consisted of two outer current probes and two inner voltage probes. The resistance R refers to the sample resistance between the inner probes. The four electrical contacts were around the whole perimeter of the sample in four parallel planes that were perpendicular to the stress axis, such that the inner probes were 60 mm apart and the outer probes were 80 mm apart. A resistive strain gauge was attached to the center of one of the largest opposite faces for measurement of strain in the stress direction. A Keithley 2001 multimeter was used for direct-current (dc) resistance measurement. The displacement rate was 1.0 mm/min, as provided by a hydraulic mechanical testing system (MTS 810). Tension–tension fatigue testing was performed with stress ratio (minimum stress to maximum stress in a cycle) 0.05 and maximum stress 740 MPa (at which strain = 0.56%). The fatigue test was run at a constant amplitude load level (load control). Each cycle took 1 s. For the fatigue data presented in this paper, a total of 396,854 cycles took place before fatigue failure. Although the fatigue data for one sample are shown in Sec. III. B of this paper, three samples were tested to confirm that the results presented here concerning the pattern of changes in resistance, stress, and strain during fatigue (not the fatigue life) are reproducible. The data shown are not the average of the data of the three samples. Among the results for the three samples, the spread in the number of cycles at failure was ±2000 cycles and the spread in the number of cycles at the start of fiber breakage was ±800 cycles.

The Poisson ratio was measured by applying two perpendicular strain gauges on each specimen (one gauge in the stress direction and the other gauge perpendicular to the stress, with both gauges on the largest surface of the specimen). The fiber volume fraction, density, and mechanical and electrical properties, as measured in this work, are listed in Table II. That the tensile strength is lower than that calculated by the Rule of Mixtures is due to the fiber waviness and imperfect fiber alignment, which were partly inherent to the fiber prepreg and partly produced during the resin flow in the process of composite laminate fabrication. The fiber volume fraction of 58% corresponds to having 38 fiber bundles in a tensile specimen.

TABLE I. Carbon-fiber and epoxy-matrix properties (according to ICI Fiberite).

10E–Torayca T-300 (6K) untwisted, UC-309 sized	
Diameter	7 μm
Density	1.76 g/cm^3
Tensile modulus	221 GPa
Tensile strength	3.1 GPa
976 Epoxy	
Process temperature	350 °F (177 °C)
Maximum service temperature	350 °F (177 °C) dry 250 °F (121 °C) wet
Flexural modulus	3.7 GPa
Flexural strength	138 MPa
T_g	232 °C
Density	1.28 g/cm^3

III. RESULTS AND DISCUSSION

A. Static loading

Figure 1(a) shows the tensile stress, strain, and fractional change in electrical resistance $\Delta R/R_o$ in the stress direction (0°) obtained simultaneously during static tensile loading up to failure. The longitudinal $\Delta R/R_o$ first decreased until 0.5% strain. The decrease is due to in-

TABLE II. Properties of carbon-fiber epoxy-matrix composite.

Volume fraction of fiber (%)	58
Density (g/cm^3)	1.52 ± 0.01
Tensile strength (MPa)	1268 ± 89
Tensile strain (%)	1.08 ± 0.08
Poisson ratio	0.30
Resistivity (Ω cm)	
0°	4.1×10^{-3}
Through thickness	2.04

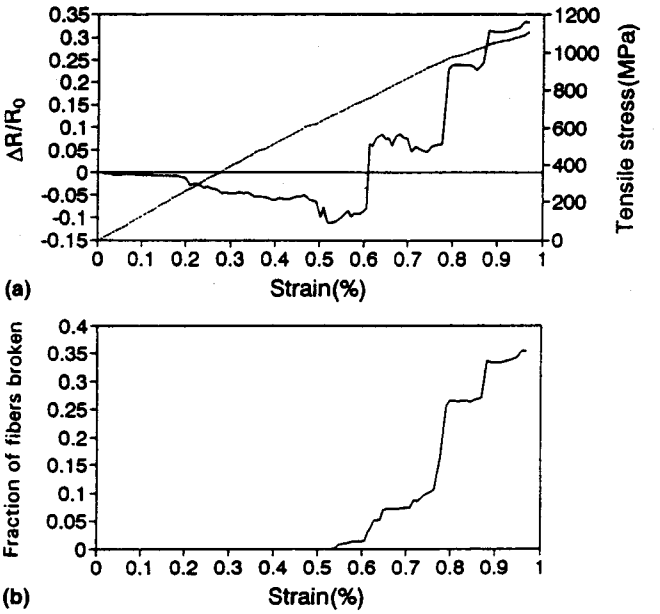

FIG. 1. (a) Tensile stress, strain, and $\Delta R/R_o$ in the 0° direction of composite, obtained simultaneously during static 0° tension up to failure. Solid curve: $\Delta R/R_o$ versus strain. Dashed curve: tensile stress versus strain. (b) Fraction of fibers broken (lower bound) versus strain during 0° tension of composite.

crease in the degree of fiber alignment upon loading and decrease in the residual compressive stress in the fiber upon loading, as supported by the increase of the through-thickness resistance during loading[2] and decrease of the resistivity of a single carbon fiber embedded in epoxy upon loading.[3] Starting at 0.6% strain, the resistance increased in a stepwise fashion, due to spurts of fiber breakage. Accompanying the resistance increase was a slight decrease of the tangent modulus [slope of the stress-strain curve in Fig. 1(a)]. That the modulus decrease was slight is because broken fibers still served as a reinforcement, although not as effectively as the unbroken fibers. Thus, the modulus is not a sensitive indicator of the extent of fiber breakage. On the other hand, the electrical resistance is.

Single fibers obtained by dissolving away the polymer from the carbon-fiber prepreg were subjected to cyclic tension and simultaneous electrical resistance measurement.[3] The resistance R of a single fiber increased upon tension partly reversibly, such that, at a tensile stress equal to 83.0% of the fracture stress, the reversible portion of $\Delta R/R_o$ (due to dimensional change) was 18.4×10^{-3}, whereas the irreversible portion of $\Delta R/R_o$ (due to damage) was 4.0×10^{-3}.[3] We therefore assume that a fiber prior to breakage has an irreversible $\Delta R/R_o$ of 4.0×10^{-3}. There are two sources of irreversible $\Delta R/R_o$, namely fiber damage and fiber breakage, although the former was almost negligible compared to the latter. The irreversible $\Delta R/R_o$ due to fiber damage was subtracted from the measured $\Delta R/R_o$ [in the high-strain part of Fig. 1(a) in which $\Delta R/R_o$ had shown an increase from the minimum value] in order to obtain the irreversible $\Delta R/R_o$ due to fiber breakage.

A broken fiber can contribute to electrical conduction due to the contact between a broken fiber and an adjacent fiber. Hence, the fraction of fibers broken obtained under the assumption that a broken fiber does not contribute to electrical conduction is actually a lower bound of the fraction of fibers broken. The difference between this lower bound and the true value depends on the extent of fiber–fiber contact. In the high-strain part of Fig. 1(a) in which R had shown an increase from the minimum value R'_o,

$$\text{lower bound of fraction of fibers broken} = \frac{Q}{1+Q}\ , \qquad (1)$$

where $Q = (R - R'_o/R'_o) - 4.0 \times 10^{-3}$ and 4.0×10^{-3} is the contribution from fiber damage. Figure 1(b) shows a plot of the lower bound of the fraction of fibers broken as a function of strain, as obtained by using Eq. (1). Fiber breakage started to occur at a strain of 0.54%, which is about half of the strain at failure. (Reference 7 also reported that fiber breakage started at about half of the strain at failure.) Failure occurred when 35% (lower bound) of the fibers were broken.

If all the fibers in the composite were identical and exactly straight and parallel, all the fibers would have broken at the same strain. The observation that the strain at which fibers broke ranged from about 50% to 100% of the composite failure strain cannot be totally accounted for by the spread in fiber strength shown by single-fiber tensile testing.[3] That the fibers were not exactly straight or parallel must contribute significantly to accounting for this observation.

B. Fatigue testing

Figure 2 shows $\Delta R/R_o$, tensile stress, and tensile strain simultaneously obtained in the stress (0°) direction during cyclic tension–tension loading. The resistance R de-

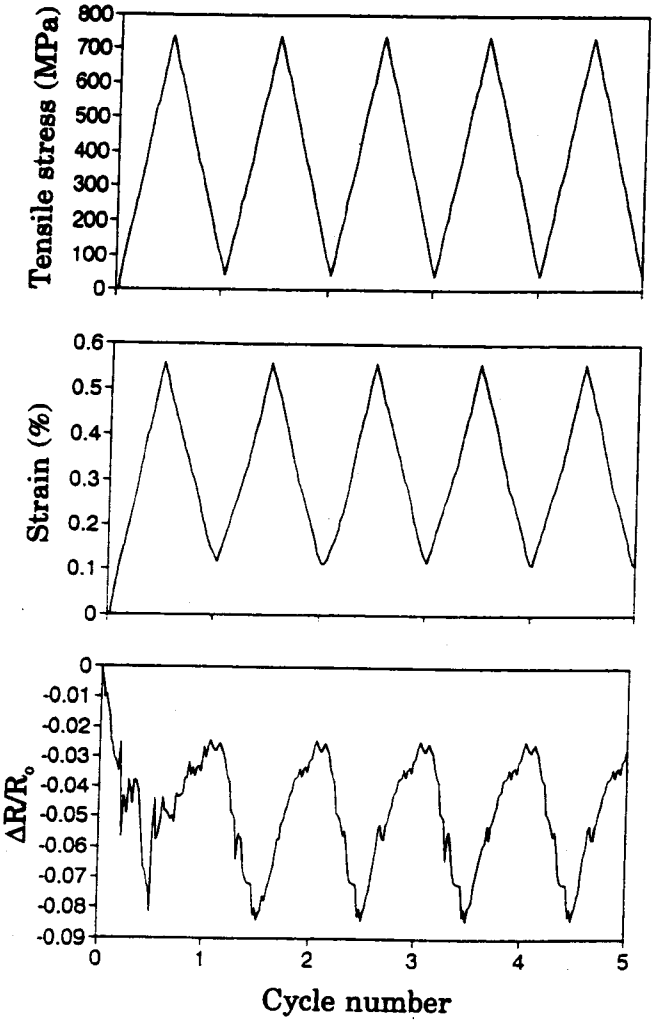

FIG. 2. Variation of fractional resistance increase ($\Delta R/R_o$), tensile stress, and tensile strain with cycle number during the first few cycles of tension–tension fatigue testing.

creased upon loading and increased upon unloading. The resistance decrease upon loading is as observed during static loading.

The resistance change in the stress direction is shown in Fig. 3 for the whole fatigue life. Figure 4 depicts the variation of peak $\Delta R/R_o$ (at the end of a cycle) as a function of the percentage of the fatigue life. No appreciable resistance change was observed from the beginning to about 48% of fatigue life, as shown in Fig. 4(a). As cycling progressed beyond 218,277 cycles (or 55% of fatigue life), the peak $\Delta R/R_o$ significantly but gradually increased, such that the resistance increase did not occur in every cycle, but occurred in spurts [Figs. 3(c), 3(d), and 4(a)], e.g., at 218,278 cycles [Fig. 3(c)] and 229,628 cycles [Fig. 4(d)]. Beyond 353,200 cycles (91% of the fatigue life), the increase of the peak R occurred continuously from cycle to cycle rather than in spurts [Fig. 3(e)]. At 396,457 cycles (99.9% of the fatigue life), the resistance increase became even more severe, such that spurts of increase occurred on top of the continuous increase [Fig. 4(b)]. The severity kept increasing until the specimen failed at 396,854 cycles, at which R abruptly increased. The last spurt observed before the final abrupt increase occurred at 396,842 cycles [Fig. 3(e)].

The normalized secant modulus of the composite during the fatigue loading is shown versus fatigue life in Fig. 5, together with the variation of the peak $\Delta R/R_o$. Both 0° resistance and 0° stiffness are sensitive to the fracture of the 0° fibers. However, the fractional change in resistance is much larger than that in stiffness.

The resistance increase and stiffness decrease during fatigue loading took place in three stages, as shown in Fig. 5. The first stage was from the beginning of the fatigue loading to about 48% of fatigue. No stiffness reduction or resistance change were observed in this stage. The second stage was from 48% to 77% of fatigue

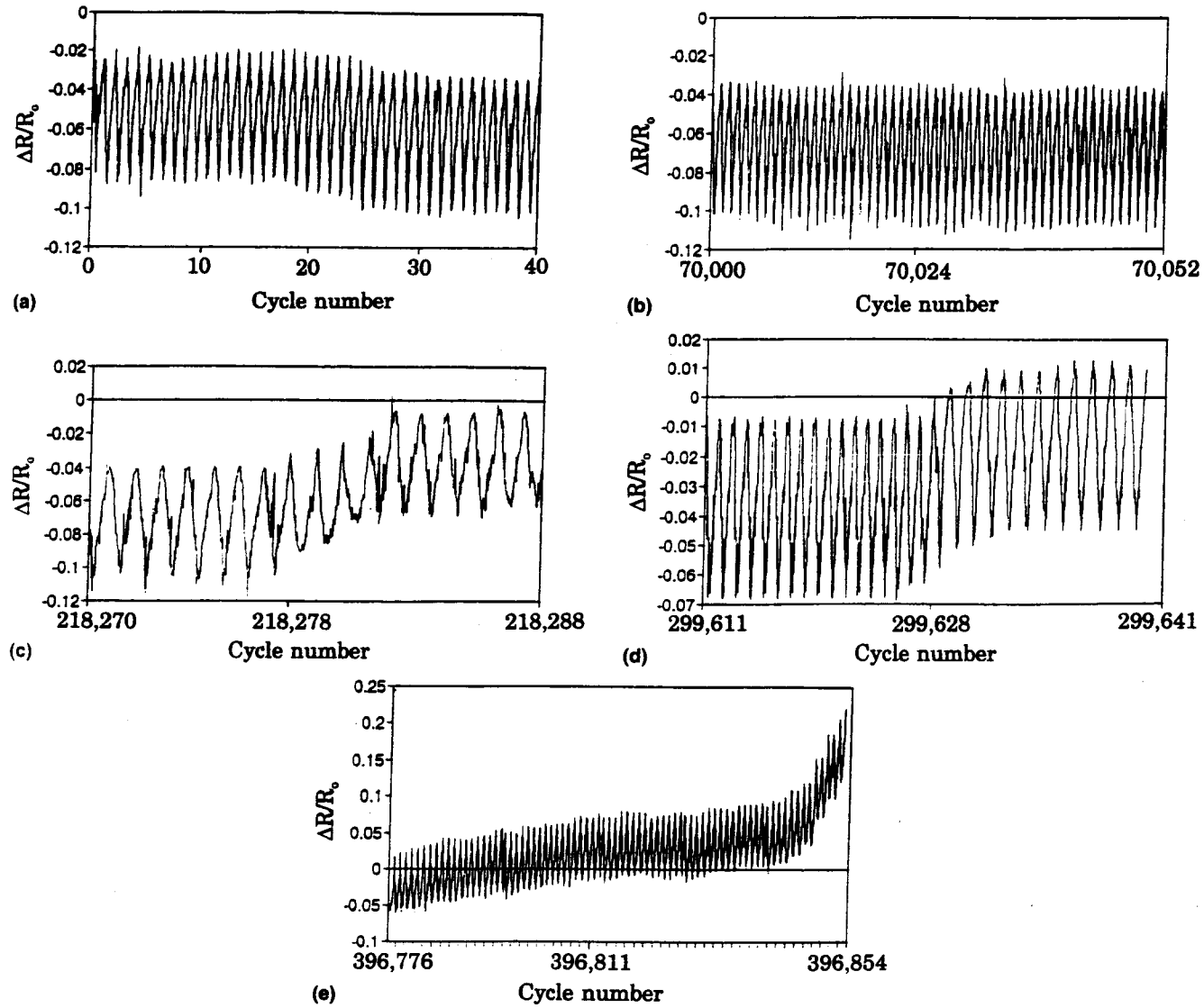

FIG. 3. Variation of $\Delta R/R_o$ with cycle number during tension–tension fatigue testing up to failure at 396,854 cycles.

life, which was characterized by increase of peak $\Delta R/R_o$ in spurts and continuous decrease in stiffness. The third stage was from 77% of fatigue life to failure. In this stage, the peak $\Delta R/R_o$ increased both in spurts and continuously and the stiffness decreased in a stepwise manner.

The absence of stiffness reduction or resistance change in the first stage indicates that no fiber fracture occurs. In the second stage, the peak $\Delta R/R_o$ increased in spurts and the stiffness decreased, suggesting that damage in the form of fiber breakage occurred. The fiber fracture was also suggested by the measured stiffness reduction of about 4.4% at the end of the second stage. The third stage (from 77% of fatigue life to failure), in which the peak $\Delta R/R_o$ increased sharply, both in spurts and continuously, and the stiffness decreased in stepwise mode, imply that more fiber breakage occurred.

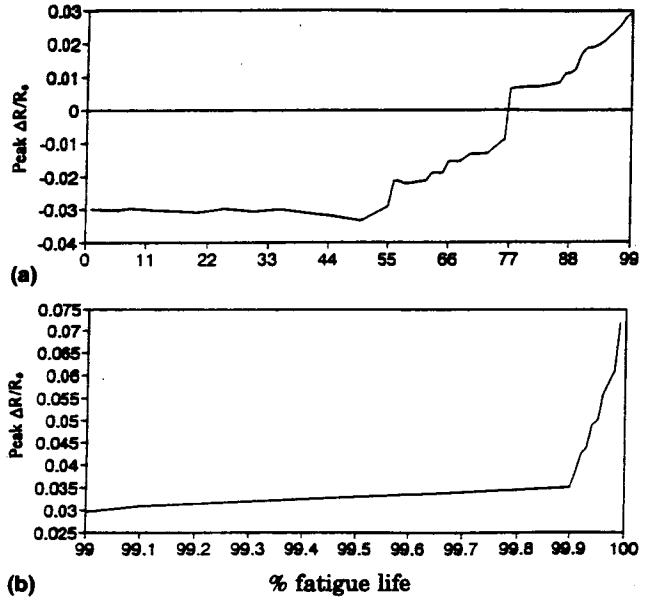

FIG. 4. Variation of the peak $\Delta R/R_o$ at the end of a cycle with the percentage of fatigue life during tension–tension fatigue testing up to failure.

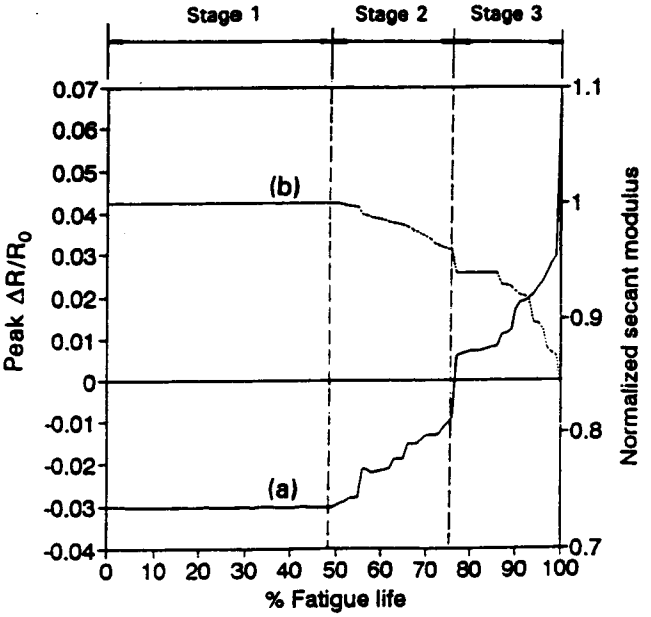

FIG. 5. (a) Peak $\Delta R/R_o$ and (b) normalized secant modulus at the end of a cycle with the percentage of fatigue life during tension–tension fatigue testing up to failure.

Fiber fracture, as indicated by resistance increase during cyclic loading in this work, had been observed by other investigators after (not during) similar cyclic loading using scanning electron microscopy.[4,5] It is known that fiber fracture and matrix cracking are dominant failure mechanisms for unidirectional composites during fatigue.[6] Because the matrix is electrically insulating and is not the major load carrier, the resistance change and stiffness reduction are related to fiber fracture only. The observed spurts of increase of the peak $\Delta R/R_o$ imply that fiber breakage occurred in spurts as the cyclic loading progressed. Fiber failure was predicted by mechanics of the stress redistribution.[7] Because most of the load is carried by the fibers, significant stress redistribution occurs due to the fiber breakage. Fiber fracture and fiber-matrix debonding contribute to the resistance increase and the stiffness reduction.

By following the change in the peak $\Delta R/R_o$, the degree of fiber fracture in the composite can be monitored progressively in real time. Moreover, progressive warning of the impending fatigue failure is provided in real time, so that the disasters caused by fatigue failure can be avoided. In the part of the fatigue life in which the peak R at the end of a cycle had shown an increase from its value R_o' at the end of the first cycle, $R_o' = R_o + (\Delta R)_o$, where R_o is the initial resistance and $(\Delta R)_o$ is ΔR at the end of the first cycle, Eq. (1) applies, with $Q = [(R - R_o')/R_o'] - 4.0 \times 10^{-3}$, R is peak R at the end of a cycle, and 4.0×10^{-3} is the contribution from fiber damage. Figure 6 is a plot of the lower bound of the fraction of fibers broken as a function of the percentage of fatigue life. Fiber breakage started at 50% of the fatigue life, although appreciable increase of the fraction of fibers broken did not start till 55% of the fatigue life. Fiber breakage occurred in spurts from 55% to 89% of the fatigue life, due to the stress distribution among the unbroken fibers. The smallest spurt involved 0.006 (lower bound) of the fibers breaking. This corresponded to 1020 broken fibers (lower bound). Thus, each spurt involved the breaking of multiple fibers (lower bound). This was reasonable because the fibers were in bundles of 6000 fibers. The smallest spurt involved the breaking of a fraction of a fiber bundle. At 89% of the fatigue life, fiber breakage started to occur continuously rather than in spurts. Catastrophic failure occurred when 18% of the fibers (lower bound) were broken.

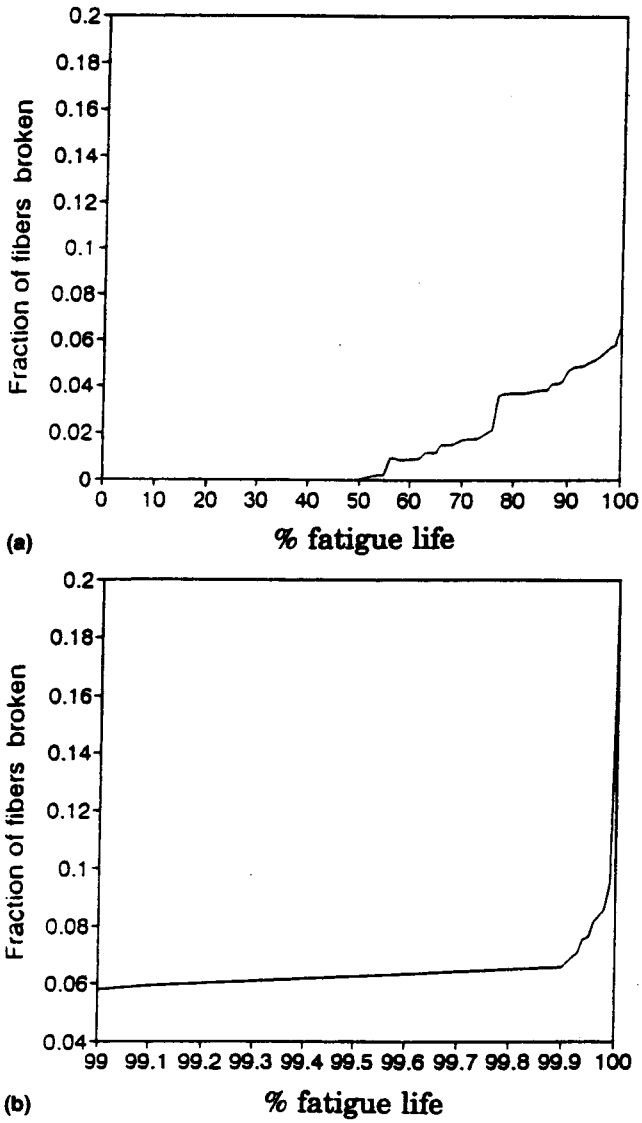

FIG. 6. Variation of the fraction of fibers broken (lower bound) with the percentage of fatigue life during tension–tension fatigue testing up to failure: (a) from 0% to 100% of fatigue life, (b) from 99% to 100% of fatigue life.

Even if all the fibers were identical and exactly straight and parallel, breakage would not have occurred at the same time for all the fibers in the composite. This is because fatigue damage tends to start at flaws and then gradually expands as dynamic loading continues. Nevertheless, it is practically useful to know that fiber breakage starts as early as 50% of the fatigue life.

Only 18% of the fibers (lower bound) were broken immediately before fatigue failure, whereas 35% of the fibers (lower bound) were broken immediately before static failure. This difference is believed to be due to the presence of accumulated damage of various types (other than fiber breakage) during fatigue. Less accumulation is expected during static loading.

IV. CONCLUSION

The evolution of fiber breakage during static and fatigue tensile loading of a continuous unidirectional carbon-fiber epoxy-matrix composite was monitored in real time by electrical resistance measurement of the composite along the fiber (stress) direction. Fiber breakage was found to occur in spurts involving 1000 fibers or more (a fraction of a fiber bundle). It started at about half of the failure strain during static loading and at about half of the fatigue life during fatigue testing. Immediately before static failure, at least 35% of the fibers were broken. Immediately before fatigue failure, at least 18% of the fibers were broken. The fiber breakage was accompanied by decrease in the modulus of the composite.

REFERENCES

1. M. Fuwa, B. Harris, and A.R. Bunsell, J. Phys. D: Appl. Phys. **8,** 1460 (1975).
2. M. Fuwa, A.R. Bunsell, and B. Harris, J. Strain Analysis **11,** 97 (1976).
3. M. Fuwa, A.R. Bunsell, and B. Harris, J. Phys. D: Appl. Phys. **9,** 353 (1976).
4. M. Fuwa, A.R. Bunsell, and B. Harris, J. Mater. Sci. **10,** 2062 (1975).
5. R.A. Badcock and G.F. Fernando, Smart Mater. Struct. **4,** 223 (1995).
6. K. Schulte, J. Physique IV, Colloque **C7,** 1629 (1993).
7. K. Schulte and Ch. Baron, Compos. Sci. Technol. **36,** 63 (1989).
8. R. Prabhakaran, Experimental Techniques **14,** 16 (1990).
9. O. Ceysson, M. Salvia, and L. Vincent, Scripta Materialia **34,** 1273 (1996).
10. N. Muto, H. Yanagida, M. Miyayama, T. Nakatsuji, M. Sugita, and Y. Ohtsuka, J. Ceramic Soc. Jpn. **100,** 585 (1992).
11. X. Wang and D.D.L. Chung, Smart Mater. Struct. **5,** 796 (1996).
12. X. Wang and D.D.L. Chung, Carbon **35,** 706 (1997).
13. N. Muto and H. Miyayama, Adv. Composite Mater. **4,** 297 (1995).
14. R.D. Jamison, Compos. Sci. Technol. **24,** 83 (1985).
15. K. O'Brien and K.L. Reifsnider, J. Testing Evaluation **5,** 384 (1977).
16. S. Steif, J. Composite Materials **17,** 153 (1984).